ACADEMIC PRESS

Available online at www.sciencedirect.com

SCIENCE DIRECT®

Journal of Magnetic Resonance 163 (2003) 149–162

JMR Journal of Magnetic Resonance

www.elsevier.com/locate/jmr

Sensitivity-enhanced phase-corrected ultra-slow magic angle turning using multiple-echo data acquisition

Jian Zhi Hu and Robert A. Wind*

Pacific Northwest National Laboratory, P.O. Box 999, MS K8-98, Richland, WA 99352, USA

Received 13 December 2002; revised 7 March 2003

Abstract

The increase in the sensitivity of the phase-corrected magic angle turning (PHORMAT) experiment at ultra-slow spinning rates by means of multiple-echo data acquisition (ME-PHORMAT) is evaluated. This is achieved by replacing the acquisition dimension in the original experiment with a train of equally spaced π-pulses. It is shown that the echoes following the odd and even π-pulses in the CPMG train must be processed differently in order to avoid spectral distortions. The method is illustrated for ^{13}C CP-ME-PHORMAT on solid 1,2,3-trimethoxybenzene and for ^{1}H ME-PHORMAT on excised rat liver tissue, both at a sample-spinning rate of 1.3 Hz. Sensitivity enhancements of a factor 4 for the solid and 2.3 for the liver were obtained. Finally, it is shown that with ME-PHORMAT one of the two RF pulse sequences, in standard PHORMAT used to obtain a pure absorption mode 2D spectrum, can be eliminated, thus reducing the usually long measuring time by a factor 2.

Keywords: PHORMAT; Magic angle turning; Magic angle spinning; Ultra-slow spinning; Sensitivity enhancement

1. Introduction

It is well known that in systems where the NMR linewidths are for a major part inhomogeneously broadened, a spin-echo train can be obtained in time domain by applying a Carr–Purcell–Meiboom–Gill (CPMG) RF π-pulse sequence after an excitation pulse, and that the resulting enhanced signal information can be used to enhance the NMR sensitivity per unit measuring time. This approach has been used, e.g., in MRI and in solid-state NMR of quadrupolar nuclei. In MRI the decay of the water signal after an excitation pulse is determined by both externally applied field gradients and by a variety of other macroscopic and microscopic field inhomogeneities such as the external field inhomogeneity and magnetic susceptibility gradients arising at the boundaries of cellular structures, tissue structures, organ–tissue, organ–air, and body–air interfaces [1], which can all be refocused with a π-pulse. The echoes have been used to sample more than one line in *k*-space, thus reducing the MRI measuring time [2]. Examples of such techniques are rapid acquisition with relaxation enhancement (RARE) imaging [2] and echo-planar imaging (EPI) [3]. In solid state NMR of integer and half-integer quadrupolar nuclei CPMG has been used successfully to enhance the signal-to-noise ratio of a single acquisition [4–7]. As the first- and second-order quadrupolar interactions often give rise to very fast decays, the spacing between the refocusing π-pulses can be made much shorter than the time constant T_e governing the decay of the echo envelop. The result is that many echoes are observed, tens or more, and a significant increase in sensitivity, an order of magnitude or more, is obtained [6,8]. The method has been applied in combination with both standard and multiple-quantum quadrupolar NMR and without and with magic angle spinning (MAS) [4–11]. In all cases the resulting decay (in case of MAS the decay governing the rotational echo's), observed during the acquisition time, is determined by a residual time-independent quadrupolar interaction that can be refocused by a π-pulse.

In solid-state NMR of spin 1/2 nuclei the multiple echo (ME) approach to increase the NMR sensitivity

* Corresponding author. Fax: 1-509-376-2303.
E-mail address: robert.wind@pnl.gov (R.A. Wind).

1090-7807/03/$ - see front matter © 2003 Elsevier Science (USA). All rights reserved.
doi:10.1016/S1090-7807(03)00103-4

has received much less attention. Here the spectral information is usually determined by the isotropic and anisotropic chemical shift interactions. In a static sample both interactions are refocused by a π-pulse, so CPMG works well when the time between two successive π-pulses is small compared with T_e. However, in static samples the spectra often consist of complicated patterns of overlapping chemical shift anisotropies, which makes the spectra difficult to analyze. Therefore, in almost all standard experiments MAS is applied to eliminate the chemical shift anisotropy, and the resulting rotational-echo decay is analyzed. If the time constant T_r governing this decay is determined by interactions that can be refocused by a π-pulse then the ME method still works by making the time interval between the π-pulses large compared to T_r. This situation may arise, e.g., in amorphous solids where a large, continuous dispersion of isotropic chemical shifts may occur. However, usually the decay of the spin-echo train is governed by the intrinsic spin–spin relaxation time T_2 and/or the spin–lattice relaxation time in the rotating frame, $T_{1\rho}$, which arise from time-dependent interactions that cannot be refocused by a π-pulse (the latter time constant becomes important when the effective B_1 field, generated by the pulse train, is so large that the magnetization becomes spin-locked along this field). Then no or only a weak echo is observed, resulting in at best a minimal gain in sensitivity. On the other hand, if the spacing between the pulses is reduced to values comparable to or smaller than a rotor period, the situation becomes complicated. The decay after the excitation pulse due to the anisotropic chemical shift is rendered time-dependent by the sample spinning. This time dependence is different before and after the π-pulse, resulting in an incomplete refocusing. Moreover, the π-pulse refocuses the decay due to the isotropic chemical shift as well, resulting in seriously distorted spectra.

The refocusing of the isotropic chemical shift can be avoided if a 2D experiment is applied where the isotropic decay can be determined separately from the multiple-echo decay observed in the acquisition domain. Several experiments with this property have been developed. Examples are five π magic angle turning (5-π MAT) [12a], FIREMAT) [12b], original MAT [13], and its successor, the phase-corrected MAT (PHORMAT) [14], which all are based on the magic angle hopping (MAH) experiment [15]. In these methods the decay during the evolution time is determined by the isotropic interactions, whereas the decay observed during the acquisition time is governed by both the isotropic and anisotropic interactions. Hence the acquisition dimension can be extended with a CPMG sequence without affecting the isotropic decay during the evolution time. However, a problem with 5-π MAT and FIREMAT is that the MAS frequency has to be fast compared with $(T_2)^{-1}$ in order to avoid serious signal attenuations. Since the maximum evolution time equals one rotor period, in 5-π MAT the isotropic decay becomes truncated if its decay time is longer than a rotor period, resulting in a distorted isotropic spectrum. In MAH the sample is 'hopped' over 120° during part of the evolution period, and is stationary during the acquisition time, so that a π-pulse refocuses completely the decay during this time [15,16]. However, a difficulty with MAH is the experimental realization of the intermittent hopping of the sample.

The problems associated with 5-π MAT, FIREMAT, and MAH are avoided in PHORMAT. In PHORMAT the sample is rotated continuously rather than intermittently. Moreover, in PHORMAT the spinning frequency has to be large compared to $(T_1)^{-1}$ rather than $(T_2)^{-1}$, which means that in general much lower MAS frequencies can be used than in 5-π MAT or FIREMAT [14]. Hence in this experiment the truncation in the isotropic decay during the evolution time is avoided, and the slow spinning speed makes it possible to use an unsynchronized train of π-pulses with a pulse spacing large compared to the decay time of the anisotropic interactions and small compared to the rotor period. This means that all the anisotropic information is retained and that the time dependence in the anisotropic chemical shift before and after the pulse can be neglected, so that the anisotropic decay is completely refocused. A disadvantage of PHORMAT is its intrinsic signal loss of at least a factor 4 [14], but it will be shown below that this can be compensated by the gain obtained in a ME experiment.

The purpose of this paper is fourfold: (I) A brief discussion will be given of the sensitivity gain in a CPMG experiment and the optimal way to process the echo train. (II) It will be shown that the odd and even echoes in a multiple-echo PHORMAT experiment (to be called ME-PHORMAT hereafter) need to be treated separately in order to avoid spectral distortions. Moreover, it will be shown that the even echoes can be used to replace one of the RF sequences used in standard PHORMAT, thus reducing the minimum measuring time by a factor 2. (III) The utility of ME-PHORMAT for solid-state spin 1/2 NMR will be illustrated experimentally for ^{13}C NMR using 1,2,3-trimethoxybenzene. (IV) Finally, the application of ^{1}H ME-PHORMAT spectroscopy in biological samples will be discussed. The linewidths of the NMR metabolite spectra in biological samples are for a major part broadened by magnetic susceptibility gradients [1,18,19], and it has been found that in a 7 T magnet with PHORMAT isotropic spectra are obtained with linewidths up to an order of magnitude smaller than those observed in a static experiment [17]. Moreover, spinning speeds as low as 1 Hz could be used, which makes it possible to perform PHORMAT in large biological systems, perhaps even live animals, without causing any harm by the centrifugal forces

associated with the sample spinning. In this paper results of a ^{1}H ME-PHORMAT experiment will be shown obtained on excised rat liver tissue.

2. Theory

2.1. The data handling and sensitivity gain in a ME experiment

The echo train can be analyzed in two ways [6,8], which are illustrated in Fig. 1.

(i) By Fourier transforming (FT) the echo train as measured. Then a so-called spikelet spectrum is observed, consisting of a series of sharp intensities with a width determined by the time constant T_e characterizing the decay of the echo envelop, separated by a frequency equal to the inverse time between two successive refocusing π-pulses, and with an intensity distribution determined by the inhomogeneous line shape, see Fig. 1a. This will be called the spikelet method.

(ii) By separating all signal transients before and after the echo maxima, negating the sign of the imaginary parts of the transients before the echo maxima, inverting the real and imaginary parts in time, shifting the resulting decays in time so that they all start at $t = 0$, and adding them together. Then after FT the full spectrum is obtained, see Fig. 1b. This will be called the superposition method.

In general the superposition method provides the best results. In order to clarify this we consider a time-dependent signal consisting of a signal decay $G_0(t)$ and a noise transient with a standard deviation n_0 after the first excitation pulse, followed by a train of N echoes, decaying with a time constant T_e that can be determined by the intrinsic T_2, $T_{1\rho}$, and, for biological samples and other systems containing mobile molecules and internal magnetic gradients, by the diffusion of the molecules in these gradients [17,20,21]. We assume that $G_0(t)$ decays with a characteristic time T_2^* much shorter than the acquisition time τ, so that this decay is not truncated. Finally, it is assumed that Nyquist's sampling theorem is fulfilled, hence that the spectral width is equal to or less than the width of the audio filter, i.e., less than twice the cutoff frequency of this filter. It follows:

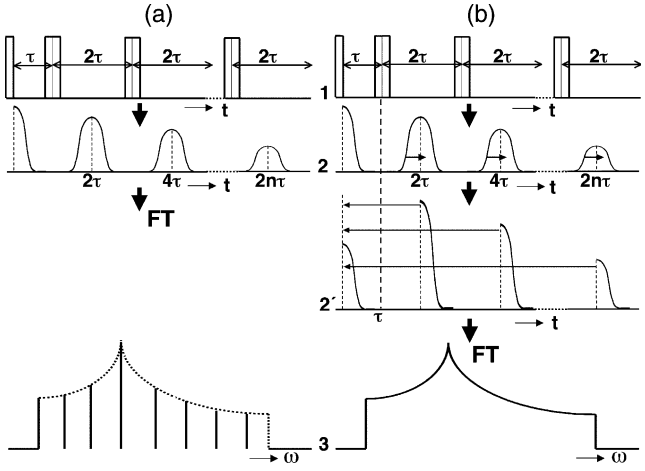

Fig. 1. Illustration of processing the signal acquired in a conventional 1D CPMG sequence using the spikelet method (a) and the superposition method (b). (a1) The CPMG sequence; (a2) the echo train; (a3) the spikelet spectrum; (b1) the CPMG sequence; (b2) the transients before and after an echo are separated, the transients before the echo are inverted in time, and the sign of the imaginary FID is negated; (b2′): the starting points of all decays are shifted to $t = 0$ and added; (b3) the full spectrum.

2.1.1. The superposition method

For reasons of simplicity we ignore the effects of the finite widths of the RF pulses and the impact of T_e during each signal transient before and after an echo. Then the resulting signal in time domain is enhanced by a factor $[1 + 2\sum_{n=1}^{N} \exp(-2n\tau/T_e)]$, and the resulting frequency spectrum $F_1(\omega)$ is given by

$$F_1(\omega) = \sum_{i=0}^{N} F_i(\omega) = F_0(\omega)\left[1 + 2\sum_{n=1}^{N} \exp(-2n\tau/T_e)\right], \quad (1)$$

where $F_0(\omega)$ is the Fourier transform of $G_0(t)$. The noise in time domain is enlarged by a factor $\sqrt{(1+2N)}$, and the noise in frequency domain is enlarged by the same factor. Hence the use of N echoes results in a sensitivity gain, G_1, both in time and frequency domain, given by

$$G_1 = \frac{1 + 2\sum_{n=1}^{N} \exp(-2n\tau/T_e)}{\sqrt{(1+2N)}}. \quad (2)$$

In Fig. 2 the sensitivity gain G_1 is given as a function of N for different values of the ratio $T_e/2\tau$. It follows

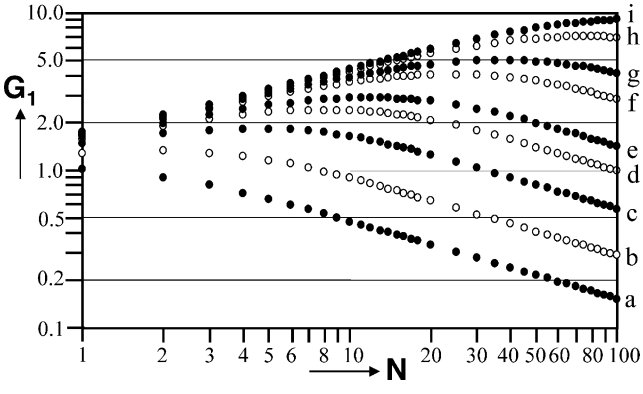

Fig. 2. The sensitivity gain, G_1, as a function of the number of echoes (N) for different values of the ratio $T_e/2\tau$ in a conventional 1D CPMG experiment, where the data are processed with the superposition method. The values of $T_e/2\tau$ are: 1 (a), 2 (b), 4 (c), 7 (d), 10 (e), 20 (f), 30 (g), 60 (h), and 100 (i), respectively.

that as a rule of thumb G_1 becomes maximal when the amount of echoes approximately equals $T_e/2\tau$, which means that the last echo amplitude that needs to be taken into account is approximately a factor $1/e$ less than that of the first decay $G_0(t)$. It is worth noting that the same result is obtained if the pre-echo transients are time inverted but the sign of their imaginary parts is not negated, and processed separately. By shifting them in time so that they all start at $t = 0$ and adding them together, after Fourier transformation a spectrum is obtained where the direction is inverted compared to the spectrum obtained from the post-echo transients. Hence by inverting the direction of one of the spectra both spectra can be added, and the resulting sensitivity gain is given by Eq. (2) again. This method is sometimes easier to perform with the existing spectrometer software than the operation of both inverting and negating the imaginary parts of the pre-echo transients in time domain.

2.1.2. The spikelet method

The decay after the nth echo, $G_n(t)$, is given by $G_n(t) = G_0(t - 2n\tau)\exp(-2n\tau/T_e)$. Hence compared to G_0(t) this decay is delayed by a time $2n\tau$, which after FT introduces a first-order phase shift in the corresponding frequency spectrum $F_n(\omega)$: $F_n(\omega) = \exp(-i\omega 2n\tau)F_0(\omega)\exp(-2n\tau/T_e)$. The total signal in frequency domain, $F_{t2}(\omega)$, is given by

$$F_{t2}(\omega) = \sum_{i=0}^{N} F_i(\omega) = F_0(\omega) \times \left[1 + 2\sum_{n=1}^{N} \exp(-i2\omega n\tau)\exp(-2n\tau/T_e)\right]. \quad (3)$$

It follows that the frequency spectra of the various echoes contain oscillatory terms that interfere with each other. This reduces the overall signal intensity except when $\exp(-i2\omega n\tau) = 1$, resulting in the spikelet spectrum described above. It follows from Eqs. (1) and (3) that the signal intensity is the same for both methods when $\exp(-i2\omega n\tau) = 1$, but that the integrated signal intensity is considerably larger when the superposition method is applied. This difference in integrated intensities arises from the fact that the integrated intensity of a spectrum in frequency domain equals the initial value of the corresponding decay in time domain. In the superposition method the signal in time domain and, henceforth, the integrated signal intensity in frequency domain are enhanced. However, in the spikelet method the untreated echo train is used and the decay amplitude at $t = 0$ is the same as that observed when only the excitation pulse is applied, resulting in an unaltered integrated signal intensity. Hence the signal increase at the spikelet maxima must necessarily be accompanied by a signal decrease between the spikelets. The standard deviation of the noise of the echo train in time domain is the same as that observed after the first excitation pulse, i.e., it is a factor $\sqrt{(1 + 2N)}$ smaller than the time-domain noise observed after the data manipulation used in the superposition method. However, after FT the noise is the same for both methods, because the noise in frequency domain is proportional to the square root of the acquisition time, which is a factor $(1 + 2N)$ larger for the full echo train than the acquisition time τ obtained after adding the transients in time domain. Hence here the sensitivity gain G_2, obtained with the spikelet method, is given by

$$G_2 = \frac{1 + 2\sum_{n=1}^{N} \cos(2\omega n\tau)\exp(-2n\tau/T_e)}{\sqrt{(1 + 2N)}}, \quad (4)$$

taking the real part of the signal given in Eq. (3). It follows from Eqs. (2) and (4) that this sensitivity gain is the same as that obtained with the superposition method at the spikelet maxima, and reduced elsewhere. Also, the gain becomes maximal for the same value of N as found in the superposition method. This means that for smaller values of N the echo decay becomes truncated, resulting in a distorted spikelet spectrum. In principle damping the echo train can solve this problem. However, this causes the spikelet lines to broaden, often to such an extent that the overall sensitivity gain is reduced.

The fact that the integrated signal intensity is not increased when the data are processed with the spikelet method has for a 2D experiment like PHORMAT the important consequence that the signal-to-noise ratio of the isotropic spectrum is often not enhanced as well. Here the isotropic spectrum is obtained by projecting both the anisotropic signal and the noise within the frequency range containing the anisotropic spectrum onto the isotropic axis. It follows from the above that for the superposition method the sensitivity gain of the isotropic lines is still given by Eq. (2). However, for the spikelet method the sensitivity gain in the isotropic spectrum depends on the $T_e/2\tau$ value. For large values of $T_e/2\tau$ many echoes are observed and most or all of the spin-echo decay can be used to optimize the sensitivity. Then the spikelet spectrum consists of relatively sharp lines with a width determined by T_e^{-1}, which are well separated from each other. In this case only the spikelets and the noise present within the spectral areas encompassing the spikelets need to be projected, whereas for the superposition method the total noise within the full anisotropic spectral width needs to be used. Hence in the spikelet case the isotropic noise becomes a factor of the order of $\sqrt{T_e/2\tau}$ smaller than the isotropic noise resulting from the superposition method, and similar sensitivity gains may be obtained with both cases. However, for smaller values of $T_e/2\tau$, where only a few echoes need to be used, the spikelets become distorted or broadened if a damping in the echo train is applied. In

this case the anisotropic spectrum contains usually partially overlapping spikelets, and both the total anisotropic signal and the noise within the full anisotropic spectral width need to be projected. As a consequence, in this case the ME approach does not provide any sensitivity gain of the isotropic spectrum. We conclude that for ME-PHORMAT the superposition method is the method of choice to process the data, also because the full anisotropic signal information is retained.

2.2. The ME-PHORMAT experiment

Two variants of ME-PHORMAT have been used. In the first variant ME-PHORMAT is combined with ^{1}H–^{13}C cross-polarization (CP), and this so-called ME-CP-PHORMAT experiment is applied for ^{13}C experiments in solids. The second variant is used for ^{1}H experiments in biological samples. Here the CP part is replaced by a single excitation pulse (SP), and a DANTE water suppression sequence is added. This variant will be called ME-SP-PHORMAT hereafter.

Fig. 3 shows the ME-CP-PHORMAT sequence. Compared to the original PHORMAT sequence given in [14] two modifications were made. The first modification is the addition of the CPMG sequence consisting of a train of π-pulses separated by a time equal to 2τ, in phase with the magnetization at $t_1 = t_2 = 0$. The second modification is that the rotor is evenly marked by three precision marks that are mutually 120° apart. An optical detector is used to generate TTL pulses associated with these markers, which serve as trigger pulses to synchronize the time instants labeled (I), (II), and (III) at end of the CP pulses (x_H), (x_C) and the 90° pulses ($-y$), respectively, to 1/3 of the rotor period T_r. The locations (I), (II), and (III) are delayed by the time "tau" that is equal to the sum of the duration of the initial ^{1}H 90° pulse (a) and the contact time of the CP pulses. This modification is made in order to separate the three positions (I), (II), and (III) by exactly 1/3 of the rotor period over each rotor period, thus relaxing the requirement of stable spinning over a long period of time; the only requirement is that the spinning has to be stable during one rotor evolution.

An extensive description of the standard PHORMAT experiment and the mechanism that leads to line narrowing has already been published elsewhere [14,17]. Therefore, we shall confine ourselves to a brief summary of the main features. The sequence starts with a standard cross-polarization (CP) experiment, consisting of a ^{1}H 90° pulse (a) followed by a simultaneous irradiation with the ^{1}H (x_H) and ^{13}C (x_C) CP pulses satisfying the Hartmann–Hahn condition. The CP sequence is followed by the PHORMAT sequence. Here the 90° pulses are labeled p_1, p_2, and $-y$, while the 180° pulses are labeled b_1, b_2, and b_3. The magnetization processes in the transverse plane during the periods labeled $\alpha_1, \beta_1, \Phi_1, \alpha_2, \beta_2, \Phi_2, \alpha_3, \beta_3$, and Φ_3, and is stored along the longitudinal axis during the periods labeled L; Δ is an echo delay time determined by the probe-ring-down and receiver recovery times. This echo delay significantly

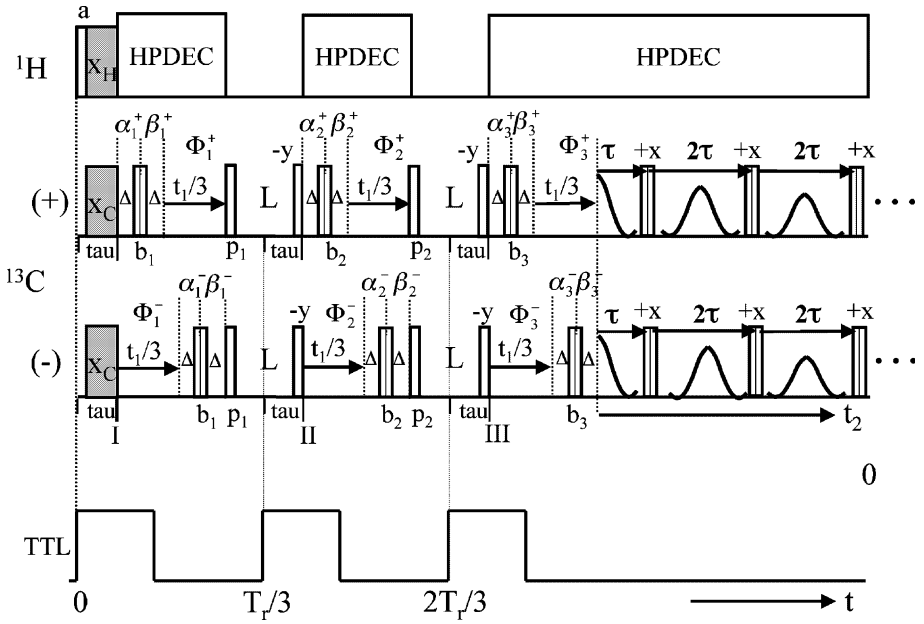

Fig. 3. The ME-CP-PHORMAT pulse sequences. 90° pulses are represented by narrow rectangles; two adjacent rectangles denote a 180° pulse. The cross-polarization pulses are shaded and have fixed phases. The phases of the receiver and pulses labeled a, p_1, p_2, b_1, b_2, and b_3 are given in Appendix A. The phases of all the π-pulses in the CPMG train are +x. The parameter Δ denotes half of the echo time along the evolution dimension for each of the triple echo segments. The bottom trace is the TTL signal generated by the optical sensor of the MAS probe.

improves the base plane of the 2D spectra, and by placing the 180° pulses b_1, b_2, and b_3 before (+) or after (−) the three phase-accumulation periods a pure absorption mode isotropic–anisotropic 2D spectrum is obtained. The pulses a, p_1, p_2, b_1, b_2, and b_3 are submitted to 32 phase cycle steps, given in Appendix A. In this way the effects of the phase accumulations of the transverse magnetization during the periods $\alpha_1, \beta_1, \alpha_2, \beta_2, \alpha_3$, and β_3 can be eliminated, retaining only the phase accumulations during the evolution periods $t_1/3$.

For ME-SP-PHORMAT following modifications were made in the sequence shown in Fig. 3: (i) The (modified) pulse sequences used for ^{13}C NMR in CP-PHORMAT are now used for ^{1}H SP-PHORMAT. (ii) The cross-polarization segment (x_C) was replaced by a 90° pulse. (iii) Immediately before the 90° pulse (−y) ending at time instant (III) a DANTE water suppression pulse sequence [22] was applied. This was achieved by switching the carrier frequency to the center of the water peak prior to the start of the DANTE sequence, and by switching this frequency back to its original value at the end of the DANTE segment. In this way the water resonance was shifted to the edge of the spectrum along the isotropic dimension of the PHORMAT sequence. As we were mainly interested in detecting the proton metabolite spectral lines with chemical shifts smaller than that of water, this makes it possible to use a reduced spectral width in the evolution dimension, resulting in a decreased number of evolution steps and, henceforth, a reduced measuring time of the experiment. (iv) The two 90° pulses occurring immediately before the time instants labeled (I) and (II) are delayed by the same time as the duration of the DANTE segment. This is done in order to separate the three 90° pulses in the PHORMAT sequence by exactly 1/3 of the rotor period T_r.

2.3. Data processing of ME-PHORMAT

A detailed discussion of the signals arising in ME-PHORMAT is given in Appendix A. It is shown that the accumulated decays obtained after phase steps 0–15 for the (+) and (−) sequences have to be stored separately from each other and from the accumulated decays obtained after phase steps 16–31. These four datasets have to be processed differently. It is also shown that the odd echoes obtained with the (+) sequence have the same phase factor as the first decay and the even echoes measured with the (−) sequence, and vice versa. Hence the odd and even echo signals in a CPMG sequence need to be processed separately, and the odd echoes in the (+) and (−) sequence need to be exchanged prior to the 2D data processing. Moreover, this result means that either the (+) or the (−) sequence may be eliminated, as, e.g., the odd echoes observed in the (+) sequence may be processed as the signals obtained with the (−) sequence. In this way the total amount of necessary phase cycles for each evolution step, and hence the minimum measuring time, can be reduced by a factor 2, which is important, as usually it takes several hours to complete a standard PHORMAT experiment.

Four methods were employed to process the data:

(a) *The spikelet ME-PHORMAT method*, following the procedure outlined above.

(b) *The superposition split-echo ME-PHORMAT method*, where the transients before and after the echoes are separated and processed according to the procedure described above.

(c) *The superposition full-echo ME-PHORMAT method.* When many echoes occur, the dwell time in the acquisition dimension has to be made relatively large in order to avoid having to store and manipulate very large numbers of data points. This makes it difficult to precisely determine the echo maxima and separate the transients before and after an echo. In this case it is easier to shift the full echoes in time so that they all have their maximum at $t = 0$ or a constant value, add them together, and Fourier transform the full echo's rather than the decays. In this method the datasets F^+ and F^-, given by Eqs. (A.7) and (A.8), and (F^+) and (F^-), given by Eqs. (A.15) and (A.16), need to be processed differently than described in Appendix A. Here the decay of F^- along the evolution dimension is inverted in time and combined with F^+ in such as way that an echo in the t_1 domain is generated, with F^- determining the t_1-transient before the echo and F^+ the transient after the echo. Then after complex FT along both t_2 and t_1, followed by absolute value manipulation, a 2D spectrum is obtained with the same shape as that resulting from the traditional phase-sensitive hyper-complex method, with an undistorted anisotropy spectrum spectrum along the ω_2 dimension. In this procedure it is difficult to incorporate the decay during the first time τ in the acquisition dimension, as this signal does not have a counterpart at negative times. Mirroring the decay might be possible, but in practice it is easier to omit this decay altogether, as this procedure was only used when many echoes are observed, so that the first decay represents only a small fraction of the total signal information. The potential shortcoming of the absolute value manipulation is that the noise becomes positive, but this is usually not a problem.

(d) *Single-sequence ME-PHORMAT.* Here only the (+) sequence is applied, and the echoes obtained after the odd π-pulses in the (+) sequence have been used to replace the signals normally obtained with the (−) sequence. Then the data are processed further using any of the methods outlined above.

3. Experimental

3.1. General

The experiments were performed on a Chemagnetics Infinity spectrometer, operating at a proton Larmor frequency of 299.982 MHz. A standard Chemagnetics ^{1}H–^{13}C CP/MAS probe with a 7.5-mm pencil type spinner system was used, with a sample volume of approximately 220 μl. In order to spin at low frequencies, the rotor was equipped with a flat drive tip (i.e. it did not contain grooves, which are normally used to drive the rotor) and an airflow restriction was induced in the driver channel. This frequency was controlled using a commercial Chemagnetics MAS speed controller under the automated control mode. All experiments were performed at room temperature.

3.2. ME-CP-PHORMAT

For the ^{13}C ME-CP-PHORMAT experiment powdered 1,2,3-trimethoxybenzene (1,2,3-TMB), purchased from Aldrich, was used. The 90° pulse widths for both the ^{13}C and ^{1}H channels were 5.25 μs, corresponding to RF fields of 48 kHz during CP. During ^{1}H decoupling, the decoupling field strength was increased to approximately 58 kHz.

At present no theoretical evaluation has been performed of the impact of the sample spinning on the echo formation in the acquisition domain, so it is unknown what the theoretical limit is of the highest sample spinning speed that can be used in ME-PHORMAT without inducing distortions in the spectra. Instead we investigated this issue experimentally by performing ^{13}C ME-CP-PHORMAT on 1,2,3-TMB at MAS frequencies in the range 1.3–8 Hz. The echoes were processed separately and the resulting 2D spectra were compared with those obtained by processing only the first decays observed prior to the first π-pulse, i.e., obtained in a standard PHORMAT experiment. No apparent spectral degradation was observed at all MAS frequencies employed. It was decided to employ the lowest spinning frequency that could be obtained with this spinning system, i.e., 1.3 Hz. With the used speed controller the long-term frequency stability in the range 1–10 Hz is about ±0.3 Hz, which appears to be sufficient for our experiments, even when spinning at 1.3 Hz. The cross-polarization time was 2 ms, and the 2D data were collected using 150 t_1 steps, incremented by 90 μs, corresponding to a maximum evolution time of 13.5 ms and an evolution spectral width of 11.1 kHz, i.e., about 147 ppm. No signal averaging was applied, which means that the total number of acquisitions equals $150 \times 64 = 9600$. The value of τ was 500 μs. In order to suppress the dead time associated with probe-ring-down and receiver recovery, 100 μs was left blank before and after each π-pulse, leaving 400 μs for data acquisition during each τ. This time was sufficiently long to measure most of the anisotropic decay (although some truncation occurs, see below). Sixteen data points were acquired during each τ with a dwell time equal 25 μs. The spectral width corresponding to the acquisition dimension is 40 kHz, or 530 ppm. The audio filter width used was 50 kHz. It was found that for 1,2,3-TMB the time constant T_e governing the echo decay is 21 ms, hence that $T_e/2\tau = 21$. It follows from Fig. 2 that for this ratio the SNR becomes maximal when the amount of echoes $N \sim 30$, and hardly changes when N is within the range 10–60. In order to restrict the amount of data points and the ^{1}H decoupling time, 14 echoes were employed, corresponding to a total of 464 data points along the t_2 dimension. The echo time (Δ) and the recycle delay times were 50 μs and 5 s, respectively. The duration of each scan is approximately one rotor period + the recycle time ~5.7 s. Hence the total measuring time of this experiment was 15.2 h.

3.3. ME-SP-PHORMAT

The ^{1}H ME-SP-PHORMAT experiment was carried out on liver tissue, excised from Fisher 344 male rats. Prior to removing the livers the animals were sacrificed by CO_2 asphyxiation. The excised liver was snap-frozen using liquid nitrogen and stored at −80 °C until required. Prior to the measurements the liver was thawed, and a piece of about 200 mg was inserted into the rotor. Finally, one of the rotor end plugs, containing a narrow opening in the middle, was squeezed tightly onto the sample to remove residual air bubbles. For the NMR experiments a 90° pulse width of 14.5 μs was used. The DANTE water suppression sequence consisted of 2000 pulses with a width of 1.2 μs and spaced by 50 μs. A fast switching diode box was used on the RF transmitter channel to reduce the dead time associated with probe-ring-down and receiver recovery. The audio filter width was 50 kHz. The 2D data were collected using 100 t_1 steps, incremented by 600 μs, corresponding to a maximum evolution time of 60 ms and an evolution spectral width of 1.67 kHz or 5.56 ppm. No signal averaging was applied, which means that the total number of acquisitions equals $100 \times 64 = 6400$. For the liver sample a much longer τ value of 6.45 ms had to be used to preserve the full anisotropic decay. In order to suppress the dead time associated with probe-ring-down and receiver recovery, 50 μs was left blank before and after each π pulse, leaving 6.40 ms for data acquisition during each τ. The time constant T_e governing the echo decay was measured to be 42 ms. Hence for the liver sample $T_e/2\tau$ is reduced to 3.3, which according to Fig. 2 means that only 3–5 echoes need to be used to optimize the sensitivity enhancement. Two hundred fifty-six data points were acquired during each τ with a dwell time of 25 μs,

resulting in 512 data points for each full echo signal. A total of 1792 data points were acquired along t_2 dimension, so that besides the initial decay 3 full echoes are observed. The echo time (Δ) and the recycle delay times were 50 μs and 1 s, respectively. The duration of each scan is approximately 1.8 s, resulting in a total measuring time of 3.2 h.

4. Results and discussion

4.1. ^{13}C ME-CP-PHORMAT of 1,2,3-trimethoxybenzene

Fig. 4a shows the 2D contour plot along with its projections along the evolution (F_1), i.e., the isotropic, and acquisition (F_2), i.e., anisotropic, dimensions, resulting from a standard CP-PHORMAT experiment, obtained by processing only the decay during the first τ period along the acquisition dimension. The isotropic projection was obtained by summing only a band of the data containing spectral intensity, i.e., between anisotropic chemical shifts in the range 0–240 ppm. Since the spectral width for the F_2 dimension is 530 ppm, such a projection, equivalent to a digital filtering in the F_2 domain prior to the projection, increases the sensitivity of the isotropic projection by approximately 49%. Also given are the line assignments in the isotropic projection, obtained from [23]. It can be observed that the quantitative integrity of the isotropic projection is compromised, which is a result of a variety of factors such as the relatively low CP and decoupling fields employed, the finite CP contact time, and differences in the ^1H–^{13}C contact times and $T_{1\rho}$ values for the various carbons. Fig. 4b shows the powder chemical shift anisotropy (CSA) spectra of each of these lines, obtained by taking a spectral slice parallel to the F_2 axis and at the center of each resolved isotropic resonance. It follows from Fig. 4a that the isotropic projection consists of seven lines, where the resonances arising from the methoxy carbons M_1 and M_3, separated by only 1 ppm, are well resolved. This resolution, obtained at the ultra-slow spinning rate of 1.3 Hz, is similar to that obtained with fast MAS at a sample spinning rate of several kHz. This indicates that the triggering mechanism outlined in Fig. 3 works very well and the spinning rate is sufficiently stable during each rotor period to avoid broadening of the isotropic lines.

Fig. 5a shows ME-CP-PHORMAT spectra of 1,2,3-TMB obtained by utilizing the total acquisition decay consisting of the initial decay and the 14 echoes, and processing the data with the spikelet ME-PHORMAT

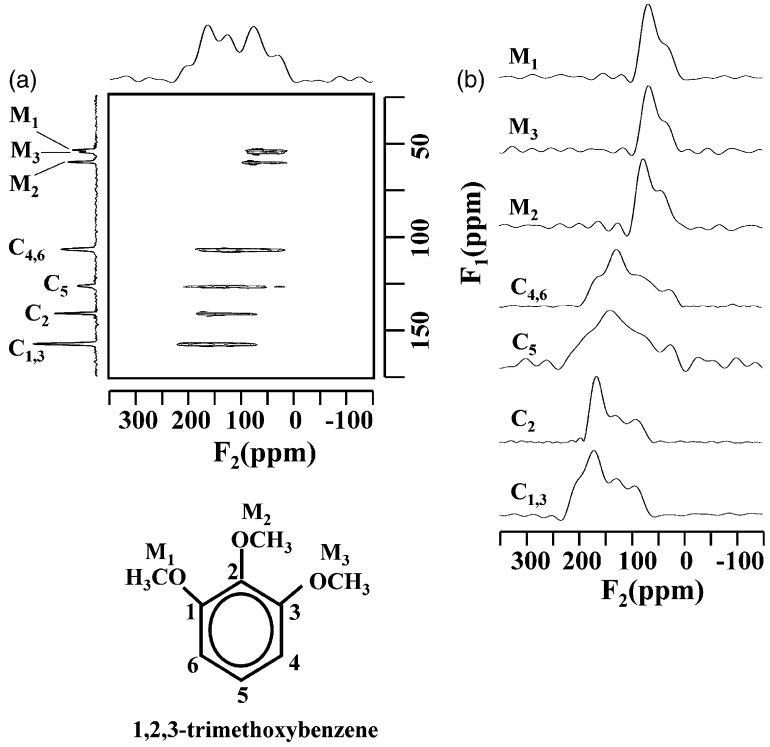

Fig. 4. ^{13}C spectra of a solid powder sample of 1,2,3-trimethoxybenzene obtained with standard CP-PHORMAT, i.e., by using the data from both the (+) and the (−) sequences during only the first τ period of the acquisition time. (a) 2D contour plot with isotropic and anisotropic projections. The isotropic projection was obtained by only summing the data between 0 and 240 ppm. The line assignment was obtained from [23]. (b) Chemical shift anisotropy (CSA) spectra of each carbon in the molecule. The amplitudes of the various spectra are scaled to the same size. The spectra were obtained by cutting slices parallel to the acquisition dimension and at the center of each resolved isotropic resonance.

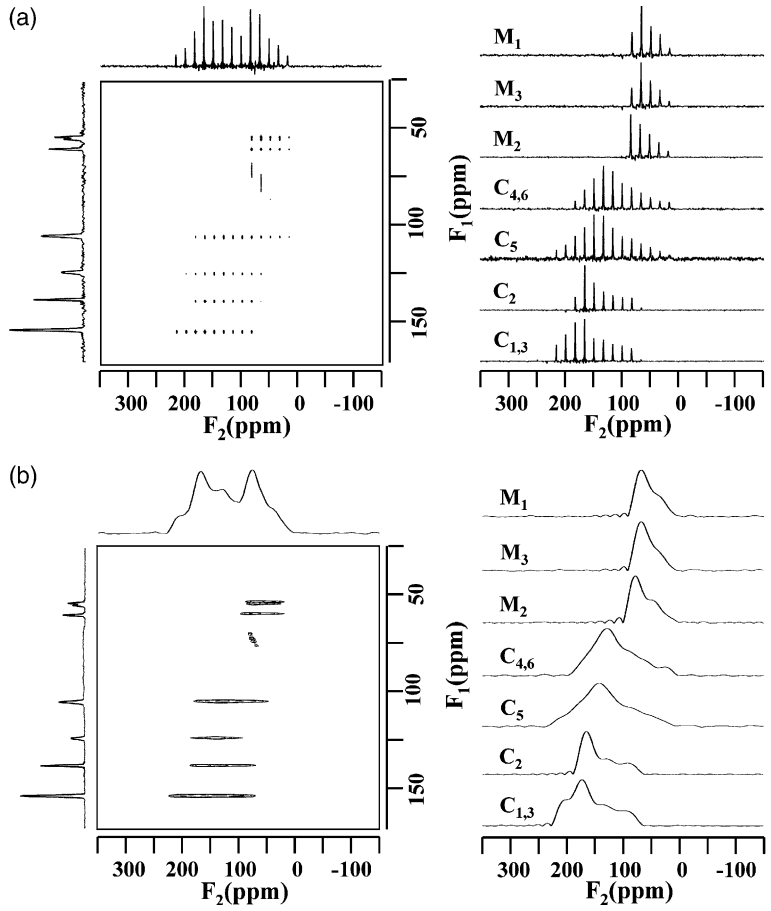

Fig. 5. (a) ^{13}C spectra of 1,2,3-TMB obtained with ME-CP-PHORMAT, using the spikelet method, processing the first decay and 14 echoes of both the (+) and (−) sequences. (b) ^{13}C ME-CP-PHORMAT spectra of 1,2,3-TMB with ME-CP-PHORMAT, using the full-echo superposition method. Here the first decay was omitted and 14 echoes of both the (+) and (−) sequences were used for the data processing.

method. The quality of the resulting 2D spectrum is good except for some low intensity artifacts around 75 ppm in the F_1 domain. At present the origin of these artifacts is unknown, and is under investigation. In the 2D plot, the CSA spikelet spectrum corresponding to each carbon is displayed along F_2 dimension. Since the intensity of the 14th echo is still about 68% of the initial signal intensity at $t_2 = 0$, the echo-train is truncated. This results in small but visible Gibbs wiggles between the spikelets, which are evident in the projection along F_2 and the individual spikelet spectra. Compared with the standard PHORMAT experiment (Fig. 4a) a significant gain in sensitivity, about a factor 4, is obtained in the spikelet spectra, in accordance with the theoretical expectations, cf. Fig. 2. However, the isotropic projection, obtained by projecting the band between 0 and 240 ppm, is identical to that shown in Fig. 4a, which is due to the fact that, as outlined above, the first data point along the t_2 dimension, which is responsible for the isotropic projection, is the same in both experiments. Hence there is no gain in the SNR of the isotropic projection if the spikelet method is used to process the data.

Fig. 5b shows the ME-CP-PHORMAT spectra of 1,2,3-TMB obtained by processing the data with the superposition method. Here the full echo method was used, because the small amount of data points during each echo made it impossible to separate the transients before and after the echo maxima accurately. As mentioned above, the signal during the first τ period along t_2 dimension had to be omitted because there is no matching transient at negative times. However, this hardly influences the sensitivity, because its contribution to the overall signal intensity is small. Compared with the results obtained from the regular PHORMAT, for the non-protonated carbons a sensitivity gain of about a factor of 4 is obtained for both the anisotropic and the isotropic projections, again in accordance with the predictions given in the theory section. Moreover, the full CSA patterns are retained, thus increasing the accuracy in determining the principal values of the CSA tensors. In some of the CSA patterns slight Gibbs wiggles are observed near the sharp edges, which are due to the truncation of the anisotropic decay. For the protonated aromatic carbons C_4–C_6 the CSA powder patterns are

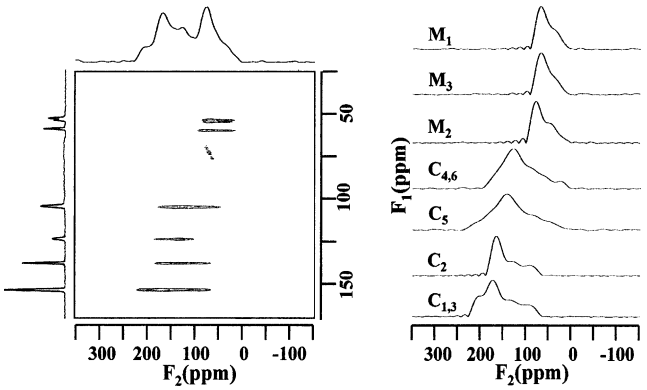

Fig. 6. ^{13}C spectra of 1,2,3-TMB obtained with ME-CP-PHORMAT, using the single-sequence ME-CP-PHORMAT experiment, processed with the full-echo superposition method. Here only the 14 echoes obtained with the (+) sequence are processed, using the even seven echoes as the (−) sequence.

distorted, i.e., the spectral intensity around the edges of the patterns are attenuated. This is caused by insufficient strengths of the RF fields applied during both CP and proton decoupling. It is known [24] that for protonated aromatic carbons, the dipolar coupling between ^{1}H and ^{13}C is the largest around the break points in the CSA patterns. Therefore, the CP fields will not completely spin-lock the carbons with strong proton couplings, and for later echoes in the CPMG echo train the signal for the carbons with strong proton coupling attenuates more than the weakly coupled or non-protonated carbons. This effect is also responsible for a reduction in the isotropic projections of the protonated carbons, reducing the sensitivity gain for these carbons to about 3. Increasing the strength of the CP and decoupling fields or employing more efficient decoupling methods [25] will improve both the quality and sensitivity gain of the ME-CP-PHORMAT experiment.

Fig. 6 shows the result of a single-sequence ME-CP-PHORMAT experiment, processed with the full-echo superposition method. Here only the 14 echoes obtained with the (+) sequence are used, employing the seven even echoes as the (−) sequence. It follows that the isotropic and CSA spectra are of the same quality as shown in Fig. 5b, and that the sensitivity obtained with single-sequence ME-CP-PHORMAT, which requires on half the measuring time of a standard experiment, is still a factor 3 larger than that obtained with standard PHORMAT, which is in agreement with the anticipated factor 2.8 (i.e., $4/\sqrt{2}$).

4.2. ^{1}H ME-SP-PHORMAT of excised rat liver tissue

The complete results of a standard SP-PHORMAT experiment, including the 2D spectrum, its anisotropic and isotropic projections, and the F_2 slices through the various metabolite lines, obtained on an excised rat liver tissue similar to the one considered in this paper, are given in [17]. It was found that the anisotropy spectra of the individual metabolite lines are similar and rather uninformative. Therefore, we shall confine ourselves to discuss the impact of multiple-echo acquisition on the SNR of the isotropic projection. Moreover, we shall only consider the superposition method, as the spikelet method leaves the SNR of the isotropic projection unaltered. In this experiment the amount of data points in the t_2 domain between two successive π-pulses was sufficiently large to accurately determine the echo maxima, allowing us to use the *superposition split-echo* ME-PHORMAT *method*. Fig. 7 shows isotropic projections obtained by processing the data in different ways. Figs. 7a–d were obtained by using both the (+) and (−) sequences, and processing only the initial decay (Fig. 7a) and the initial decay combined with one (Fig. 7b), two (Fig. 7c), and three (Fig. 7d) echoes. In Fig. 7e the isotropic projection is given, obtained by using the initial decay and three echoes of only the (+) sequence. It follows that all spectra are qualitatively the same, indicating that the 1.3 Hz sample spinning does not induce distortions in the echo transients, even though their duration is considerably longer than those in 1,2,3-TMB. In the figure also the SNR values are given corresponding to the intensity of the peak at 1.28 ppm, arising from methylene

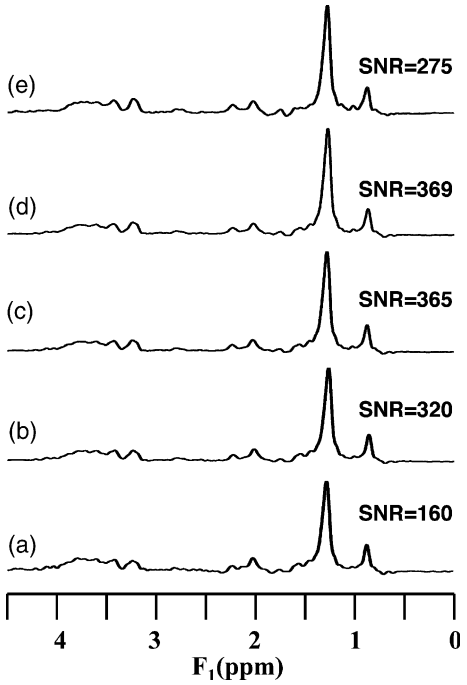

Fig. 7. ^{1}H isotropic chemical shift projection spectra of excised rat liver, obtained with different SP-PHORMAT experiments, using the split-echo superposition method for data processing. (a) Standard SP-PHORMAT, using only the first decay. (b) ME-SP-PHORMAT, using the first decay and 1 echo. (c) ME-SP-PHORMAT, using the first decay and 2 echoes. (d) ME-SP-PHORMAT, using the first decay and 3 echoes. (e) Single-sequence ME-SP-PHORMAT, using the initial decay and 3 echoes of only the (+) sequence. The SNR numbers reflect the signal-to-noise ratios of the 1.28 ppm peak, obtained with the different methods.

groups present in lipids or methyl groups present in lactate and/or threonine [17] (a full assignment of the spectrum is given in [17]). It follows that compared to standard PHORMAT the SNR is increased by a factor 2.0 when one echo is used and a factor 2.3 when 2 or 3 echoes are incorporated in the data processing. Finally, the SNR of the spectrum shown in Fig. 7e is a factor 1.7 larger than that obtained with standard PHORMAT, despite the fact the number of acquisitions is reduced by a factor 2. All these values are better than the theoretical values 1.43, 1.60, 1.65, and 1.28, predicted by Eq. (2), using the experimental value of 3.3 for the $T_e/2\tau$ ratio. The reason for this discrepancy is unknown, and is currently under investigation.

5. Conclusions

We conclude that ME-PHORMAT, combined with slow MAS frequencies, can be used successfully to improve the NMR sensitivity, provided that the data are processed in the proper way, i.e., the odd and even echoes acquired with the (+) and the (−) pulse sequences of the ME-PHORMAT experiment must be exchanged in order to process the data properly. Further it was shown that the superposition method of data processing, where the initial decay and echo signals during the acquisition time are added together prior to Fourier transformation, generally is the method of choice, as this increases the sensitivity in both the anisotropic and isotropic dimension. In contrast, with the spikelet method, where the full echo decay is used for Fourier transform (after exchanging the even echoes in the (+) and (−) sequences), results in an increase in sensitivity in only the anisotropic spectra, and leaves the SNR of the isotropic projection unaffected.

The sensitivity enhancement that can be obtained with ME-PHORMAT depends on the ratio of the isotropic and anisotropic decay times. For proton-decoupled ^{13}C PHORMAT in organic solids, where the anisotropy decay is mainly determined by the chemical shift anisotropy and is usually much faster (a factor 50 for 1,2,3-TMB) than that of the spin-echo envelope, many echoes can be obtained, resulting in a significant sensitivity enhancement. For 1,2,3-TMB at room temperature a factor 4 increase in both the isotropic and CSA spectra is obtained, and lowering the temperature together with increasing the CP and decoupling efficiency may even further increase the sensitivity. For ^{1}H PHORMAT in excised liver tissue the sensitivity enhancement is reduced, which is due to the fact that for biological samples the anisotropy decay is mainly governed by the magnetic susceptibility broadening, and is (at least for the liver sample) only a factor 6–8 faster than the decay of the echo envelope. Therefore, only a few echoes can be used. Still, by employing only two echoes the SNR was increased by a significant factor 2.3, illustrating the potential usefulness of the ultra-slow-MAS ME-PHORMAT approach to investigate biological samples, also because in other tissues and organs a substantial difference between the homogeneous and heterogeneous line broadening has been observed as well [26].

It is also possible to further improve the sensitivity of ME-PHORMAT by using a closely spaced CPMG pulse train [16], and use over-sampling combined with digital filtering to optimize the SNR. When times between the π-pulses become very short the decay of the echo envelope is governed by $T_{1\rho}$ rather than T_2, so that an increased amount of echoes can be sampled as $T_{1\rho}$ is usually larger than T_2. The disadvantage of this approach is that the anisotropic information is lost, but this may not be a serious problem for research on biological samples, where mainly the isotropic information is of interest. This possibility is currently under investigation.

Low spinning speeds have to be used in order to avoid distortions in the echo transients. Although we did not investigate this matter in depth, we estimate that the spinning speed has to be reduced to 10 Hz or less in order to avoid this type of distortions. In fact, this required use of such ultra-low spinning speeds should be regarded as an advantage, because it makes experiments possible that could not or only with great difficulty be carried out when high MAS speeds are used. For instance, it facilitates the design of many types of new measurements, where in situ controls such as temperature, pressure, and flow, are required [27–29]. Moreover, much larger samples can be used than with standard fast MAS, which further increases the sensitivity of the experiment, and last not least, ultra-slow MAS makes it possible to study large intact biological objects (perhaps even live animals) without compromising their structural integrities by the large centrifugal forces associated with large spinning speeds.

Finally, it is shown that with ME-PHORMAT the minimum amount of acquisition steps can be reduced by a factor 2, while still providing a better sensitivity than standard PHORMAT. This is a significant result, as the measuring times of a PHORMAT experiment are inherently long. In our case the measuring time for the ^{13}C experiment in 1,2,3-TMB could be reduced to 7.6 h and for the ^{1}H experiment on the liver tissue to 1.6 h. We conclude that the multiple-echo approach significantly increases the utility of ultra-slow-MAS PHORMAT for research of both solid and biological materials.

Acknowledgments

This work was supported by the Department of Energy Office of Biological and Environmental Research

Program under Grant 22342 KP-14-02-01. The research was performed in the Environmental Molecular Sciences Laboratory (a national scientific user facility sponsored by the Department of Energy's Office of Biological and Environmental Research) located at Pacific Northwest National Laboratory, and operated for DOE by Battelle. The authors gratefully acknowledge helpful discussions about the spikelet method with Dr. Paul D. Ellis.

Appendix A. Echo formation in ME-PHORMAT

In this section it will be shown that in order to correctly utilize the multiple echoes, the echo signals after the odd and even π-pulses in the CPMG sequence need to be processed separately. The phase table of the RF pulses labeled a, p_1, p_2, b_1, b_2, and b_3 of CP-PHORMAT, shown in Fig. 3, and the receiver is given in Table 1. This phase table is the same for both the (+) and (−) sequences defined in Fig. 3. For SP-PHORMAT experiment, where the top RF sequence shown in Fig. 3 is eliminated and where a 90° pulse replaces the CP segment (x_C), the phase of this pulse is the same as that of the proton RF pulse (a) in CP-PHORMAT.

In the following we shall discuss the signals obtained during the various time intervals in the acquisition domain separately. For simplicity we neglect possible signal attenuation during the evolution period due to T_1 and T_2 effects, and we assume that the spinning rate is so slow that during each acquisition period τ the sample can be considered as static, i.e., $\tau \ll T_r$, where T_r is the rotation period.

We first consider the decays obtained during the first time interval τ in the acquisition domain, i.e., the decays observed in a standard PHORMAT experiment. The accumulated decays obtained after the phase steps 0–15, to be called the real components F_R^+ and F_R^- for the (+) and (−) sequences, respectively, are stored separately from each other and from the accumulated decays obtained after phase steps 16–31, to be called the imaginary components iF_I^+ and iF_I^- for the (+) and the (−) sequences, respectively. It is shown in [14] that these four datasets are given by

$$F_R^+ = \cos(-\alpha_1^+ + \beta_1^+ + \Phi_1^+ - \alpha_2^+ + \beta_2^+ + \Phi_2^+) \times \exp(i(-\alpha_3^+ + \beta_3^+ + \Phi_3^+))F_2(t_2), \quad \text{(A.1)}$$

$$iF_I^+ = i \times \sin(-\alpha_1^+ + \beta_1^+ + \Phi_1^+ - \alpha_2^+ + \beta_2^+ + \Phi_2^+) \times \exp(i(-\alpha_3^+ + \beta_3^+ + \Phi_3^+))F_2(t_2), \quad \text{(A.2)}$$

$$F_R^- = \cos(-\alpha_1^- + \beta_1^- - \Phi_1^- - \alpha_2^- + \beta_2^- - \Phi_2^-) \times \exp(i(-\alpha_3^- + \beta_3^- - \Phi_3^-))F_2(t_2), \quad \text{(A.3)}$$

$$iF_I^- = i \times \sin(-\alpha_1^- + \beta_1^- - \Phi_1^- - \alpha_2^- + \beta_2^- - \Phi_2^-) \times \exp(i(-\alpha_3^- + \beta_3^- - \Phi_3^-))F_2(t_2), \quad \text{(A.4)}$$

Table 1
The phase table for ME-PHORMAT

Index pulse[a]	0	1	2	3	4	5	6	7	8	9	10	11	12	13	14	15	16	17	18	19	20	21	22	23	24	25	26	27	28	29	30	31
a[b]	+y	−y	+y	−y	+y	−y	+y	−y	+y	−y	+y	−y	+y	−y	+y	−y	+y	−y	+y	− y	+y	−y	+y	−y	+y	−y	+y	−y	+y	−y	+y	−y
p_1	+y	+y	−y	−y	+y	+y	−y	−y	−x	−x	+x	+x	−x	−x	+x	+x	-x	−x	+x	+x	−x	−x	+x	+x	+y	+y	−y	−y	+y	+y	−y	−y
p_2	+y	+y	+y	+y	−y	−y	−y	−y	−x	−x	−x	−x	+x	+x	+x	+x	+y	+y	+y	+y	−y	−y	−y	−y	−x	−x	−x	−x	+x	+x	+x	+x
b[c]	+x	+x	+x	+x	+x	+x	+x	+x	−x	−x	−x	−x	−x	−x	−x	−x	+x	+x	+x	+x	+x	+x	+x	+x	−x	−x	−x	−x	−x	−x	−x	−x
Receiver[d]	+x	−x	−x	+x	−x	+x	+x	−x	−x	+x	+x	−x	+x	−x	−x	+x	−y	+y	+y	−y	+y	−y	−y	+y	−y	+y	+y	−y	+y	−y	−y	+y
Receiver[d]	+x	−x	−x	+x	−x	+x	+x	−x	−x	+x	+x	−x	+x	−x	−x	+x	+y	−y	−y	+y	−y	+y	+y	−y	+y	−y	−y	+y	−y	+y	+y	−y

[a] Pulse labels are defined in Fig. 3.
[b] For SP-PHORMAT this pulse replaces the CP segments (x_C) in Fig. 3.
[c] Includes pulses b_1, b_2, and b_3.
[d] The receiver phases for indices 16–31 depend upon the relation between receiver phase and pulse phase in a particular spectrometer, and should be selected so that Eqs. (A.7), (A.8), (A.15), and (A.16) are correct. The first row of receiver phases was used in this work.

$F_2(t_2)$ is the complex 1D FID which would follow a single $\pi/2$ excitation pulse. After addition of F_R^+ and iF_I^+, and F_R^- and iF_I^-, respectively, two new datasets F^+ and F^- are obtained, given by

$$F^+ = F_R^+ + iF_I^+ = \exp(+i((\beta_1^+ + \beta_2^+ + \beta_3^+) - (\alpha_1^+ + \alpha_2^+ + \alpha_3^+) + (\Phi_1^+ + \Phi_2^+ + \Phi_3^+)))F_2(t_2), \tag{A.5}$$

$$F^- = F_R^- + iF_I^- = \exp(+i((\beta_1^+ + \beta_2^+ + \beta_3^+) - (\alpha_1^+ + \alpha_2^+ + \alpha_3^+) - (\Phi_1^+ + \Phi_2^+ + \Phi_3^+)))F_2(t_2). \tag{A.6}$$

For second-rank interactions such as the chemical shift interaction and the interactions resulting from differences in the isotropic magnetic susceptibility, $\Phi_1 + \Phi_2 + \Phi_3$ averages to the phase accumulation associated with isotropic values of the interactions, i.e., $\Phi_1 + \Phi_2 + \Phi_3 = \omega_1 t_1$, where ω_1 denotes the isotropic frequency. Similarly, $(\beta_1^+ + \beta_2^+ + \beta_3^+) = \omega_1 3\Delta$ and $(\alpha_1^+ + \alpha_2^+ + \alpha_3^+) = \omega_1 3\Delta$. Thus Eqs. (A.5) and (A.6) become

$$F^+ = \exp(+i\omega_1 t_1)F_2(t_2), \tag{A.7}$$

$$F^- = \exp(-i\omega_1 t_1)F_2(t_2) \tag{A.8}$$

Traditionally the composite FIDs F^+ and F^- are combined to form the real part F_R and the imaginary part F_I of a hyper-complex 2D FID, in which the phase information in the t_1 and t_2 domain are separated

$$F_R = \frac{1}{2}(F^+ + F^-) = \cos(\omega_1 t_1)F_2(t_2), \tag{A.9}$$

$$F_I = \frac{-i}{2}(F^+ - F^-) = \sin(\omega_1 t_1)F_2(t_2). \tag{A.10}$$

Hence after 2D Fourier transformation an absorption–absorption-phased 2D spectrum is obtained that projects an isotropic-shift spectrum with no spinning sidebands onto the evolution-dimension axis.

Next we consider the signal after the first π-pulse in the acquisition domain. This pulse inverts the parts of the signals that are dependent on the RF phase, i.e., the exponential components and the complex decay $F_2(t_2)$ in Eqs. (A.1)–(A.4). During the first time interval τ after the pulse only the decay F_2 evolves back in time, whereas the exponentials, which are independent of the acquisition time t_2, remain unaltered. Hence the four accumulated decays $(F_R^+)_1$, $i(F_I^+)_1$, $(F_R^-)_1$, and $i(F_I^-)_1$, obtained from the decays observed in the time interval τ after the first echo, is given by

$$(F_R^+)_1 = \cos(-\alpha_1^+ + \beta_1^+ + \Phi_1^+ - \alpha_2^+ + \beta_2^+ + \Phi_2^+) \times \exp(-i(-\alpha_3^+ + \beta_3^+ + \Phi_3^+))F_2(t_2), \tag{A.11}$$

$$i(F_I^+)_1 = i \times \sin(-\alpha_1^+ + \beta_1^+ + \Phi_1^+ - \alpha_2^+ + \beta_2^+ + \Phi_2^+) \times \exp(-i(-\alpha_3^+ + \beta_3^+ + \Phi_3^+))F_2(t_2), \tag{A.12}$$

$$(F_R^-)_1 = \cos(-\alpha_1^- + \beta_1^- - \Phi_1^- - \alpha_2^- + \beta_2^- - \Phi_2^-) \times \exp(-i(-\alpha_3^- + \beta_3^- - \Phi_3^-))F_2(t_2), \tag{A.13}$$

$$i(F_I^-)_1 = i \times \sin(-\alpha_1^- + \beta_1^- - \Phi_1^- - \alpha_2^- + \beta_2^- - \Phi_2^-) \times \exp(-i(-\alpha_3^- + \beta_3^- - \Phi_3^-))F_2(t_2). \tag{A.14}$$

It follows that addition of e.g., $(F_R^+)_1$ and $i(F_I^+)_1$, leads to erroneous results, as the various evolution phases α_i, β_i, and Φ_i ($i = 1, 2, 3$) no longer add up to the isotropic frequency times an evolution time. Instead, $i(F_I^+)_1$ has to be subtracted from $(F_R^+)_1$, and $i(F_I^-)_1$ has to be subtracted from $(F_R^-)_1$. Then the resulting datasets $(F^+)_1$ and $(F^-)_1$ are given by

$$(F^+)_1 = (F_R^+)_1 - i(F_I^+)_1 = \exp(-i\omega_1 t_1)F_2(t_2), \tag{A.15}$$

$$(F^-)_1 = (F_R^-)_1 - i(F_I^-)_1 = \exp(+i\omega_1 t_1)F_2(t_2), \tag{A.16}$$

and $(F^+)_1$ and $(F^-)_1$ can be combined to give a hyper-complex 2D FID again.

Following the same procedures as given above it can easily be shown that the decays after the echoes following the even π-pulses in the CPMG train are all given by Eqs. (A.7) and (A.8), whereas the decays after the echoes following the odd π-pulses in the CPMG train are all given by Eqs. (A.15) and (A.16). Moreover, it can be observed from these equations that the dataset $(F^+)_1$, obtained after the odd π-pulses, equals the dataset F^- obtained during the first time period τ and after the even π-pulses, and that the dataset $(F^-)_1 = F^+$. This means that the transients following the odd and even π-pulses need to be handled separately, and that the odd echoes observed in the (+) sequence need to be exchanged with the corresponding echoes in the (−) sequence before processing the data further. Moreover, this result means that the use of multiple echoes makes it possible to eliminate one of (+) or (−) sequences altogether, as the echo train observed with each of these sequences contains the information from the other sequence as well. Hence in this way the amount of acquisition steps, necessary to produce a hyper-complex 2D FID, can be reduced by a factor 2.

References

[1] D.A. Yablonskiy, Quantitation of intrinsic magnetic susceptibility-related effects in a tissue matrix. Phantom study, Magn. Reson. Med. 39 (1998) 417–428.

[2] J.K. Hennig, Multi echo acquisition techniques using inverting radiofrequency pulses in MRI, in: I.R. Young (Ed.), Methods in Biomedical Magnetic Resonance Imaging and Spectroscopy, Wiley, London, 2000, pp. 256–264.

[3] P. Mansfield, Echo-planar imaging, in: I.R. Young (Ed.), Methods in Biomedical Magnetic Resonance Imaging and Spectroscopy, Wiley, London, 2000, pp. 265–270.

[4] F.H. Larsen, H.J. Jakobsen, P.D. Ellis, N.C. Nielsen, Sensitivity-enhanced quadrupolar-echo NMR of half-integer quadrupolar nuclei. Magnitudes and relative orientation of chemical shielding

and quadrupolar coupling tensors, J. Phys. Chem. A 101 (1997) 8597–8606.
[5] F.H. Larsen, H.J. Jakobsen, P.D. Ellis, N.C. Nielsen, Molecular dynamics from ^{2}H quadrupolar Carr–Purcell–Meiboom–Gill solid-state NMR spectroscopy, Chem. Phys. Lett. 292 (1998) 467–473.
[6] F.H. Larsen, J. Skibsted, H.J. Jakobsen, N.C. Nielsen, Solid-state QCPMG of low-γ quadrupolar metal nuclei in natural abundance, J. Am. Chem. Soc. 122 (2000) 7080–7086.
[7] A.S. Lipton, J.A. Sears, P.D. Ellis, A general strategy for the NMR observation of half-integer quadrupolar nuclei in dilute environments, J. Magn. Reson. 151 (2001) 48–59.
[8] R. Lefort, J.W. Wiench, M. Pruski, J.-P. Amoureux, Optimization of data acquisition and processing in Carr–Purcell–Meiboom–Gill multiple quantum magic angle spinning nuclear magnetic resonance, J. Chem. Phys. 116 (2002) 2493–2501.
[9] T. Vosegaard, F.H. Larsen, H.J. Jakobsen, P.D. Ellis, N.C. Nielsen, Sensitivity-enhanced multiple-quantum MAS NMR of half-integer quadrupolar nuclei, J. Am. Chem. Soc. 119 (1997) 9055–9056.
[10] F.H. Larsen, H.J. Jakobsen, P.D. Ellis, N.C. Nielsen, High-field QCPMG-MAS NMR of half-integer quadrupolar nuclei with large quadrupolar couplings, Mol. Phys. 95 (1998) 1185–1195.
[11] F.H. Larsen, H.J. Jakobsen, P.D. Ellis, N.C. Nielsen, QCPMG-MAS NMR of half-integer quadrupolar nuclei, J. Magn. Reson. 131 (1998) 144–147.
[12] (a) J.Z. Hu, D.W. Alderman, C. Ye, R.J. Pugmire, D.M. Grant, An isotropic chemical shift-chemical shift anisotropy magic angle slow-spinning 2D NMR experiment, J. Magn. Reson. A 105 (1993) 82–87;
(b) D.W. Alderman, G. McGeorge, J.Z. Hu, R.J. Pugmire, D.M. Grant, A sensitive, high resolution magic angle turning experiment for measuring chemical shift tensor principal values, Mol. Phys. 95 (1998) 1113–1126.
[13] Z. Gan, High-resolution chemical shift and chemical shift anisotropy correlation in solids using slow magic angle spinning, J. Am. Chem. Soc. 114 (1992) 8307–8309.
[14] J.Z. Hu, W. Wang, F. Liu, M.S. Solum, D.W. Alderman, R.J. Pugmire, D.M. Grant, Magic-angle-turning experiments for measuring chemical-shift-tensor principal values in powdered solids, J. Magn. Reson. A 113 (1995) 210–222.
[15] A. Bax, N.M. Szeverenyi, G.E. Maciel, Correlation of isotropic shifts and chemical shift anisotropies by two-dimensional Fourier-transform magic angle hopping NMR spectroscopy, J. Magn. Reson. 52 (1983) 147–152.
[16] N.M. Szeverenyi, A. Bax, G.E. Maciel, Magic-angle hopping as an alternative to magic-angle spinning for solid state NMR, J. Magn. Reson. 61 (1985) 440–447.
[17] J.Z. Hu, D.N. Rommereim, R.A. Wind, High resolution ^{1}H NMR spectroscopy in rat liver using magic angle turning at a 1 Hz spinning rate, Magn. Reson. Med. 47 (2002) 829–836.
[18] F. Adebodun, J. Post, Bulk magnetic susceptibility induced line broadening in the ^{19}F NMR spectra of suspended leukemic cells, NMR Biomed. 6 (1993) 125–129.
[19] P. Weybright, K. Millis, N. Campbell, D.G. Cory, S. Singer, Gradient, high-resolution, magic angle spinning ^{1}H nuclear magnetic resonance spectroscopy of intact cells, Magn. Reson. Med. 39 (1998) 337–345.
[20] G. Leu, X. Tang, S. Peled, W.E. Maas, S. Singer, D.G. Cory, P.N. Sen, Amplitude modulation and relaxation due to diffusion in NMR experiments with a rotating sample, Chem. Phys. Lett. 332 (2000) 344–350.
[21] Y. Liu, G. Leu, S. Singer, D.G. Cory, P.N. Sen, Manipulation of phase and amplitude modulation of spin magnetization in magic angle spinning nuclear magnetic resonance in the presence of molecular diffusion, J. Chem. Phys. 114 (2001) 5729–5734.
[22] G.A. Morris, R. Freeman, Selective excitation in Fourier transform nuclear magnetic resonance, J. Magn. Reson. 29 (1978) 433–462.
[23] J.Z. Hu, A.M. Orendt, D.W. Alderman, R.J. Pugmire, C. Ye, D.M. Grant, Measurement of ^{13}C chemical shift tensor principal values with a magic angle turning experiment, Solid State NMR 3 (1994) 181–197.
[24] J.Z. Hu, D.W. Alderman, R.G. Pugmire, D.M. Grant, A high-resolution 3D separated-local-field experiment by means of magic angle turning, J. Magn. Reson. 126 (1997) 120–126.
[25] A.E. Bennett, C.M. Rienstra, M. Auger, K.V. Lakshmi, R.G. Griffin, Heteronuclear decoupling in rotating solids, J. Chem. Phys. 103 (1995) 6951–6958.
[26] R.A. Wind, J.Z. Hu, D.N. Rommereim, High resolution ^{1}H NMR spectroscopy in organs and tissues using slow magic angle spinning, Magn. Reson. Med. 46 (2001) 213–218.
[27] C. Keeler, J. Xiong, H. Lock, S. Dec, T. Tao, G.E. Maciel, A new in situ chemical reactor for studying heterogeneous catalysis by NMR: the GRASSHopper, Catal. Today 49 (1999) 377–383.
[28] M. Hunger, T. Horvath, A new MAS NMR probe for in situ investigations of hydrocarbon conversion on solid catalysts under continuous-flow conditions, J. Chem. Soc.—Chem. Commun. (1995) 1423–1424.
[29] P. Goguen, J.F. Haw, An in situ NMR probe with reagent flow and magic angle spinning, J. Catal. 161 (1996) 870–872.